Laser and Particle Beams (2013), *31*, 371–377.

doi:10.1017/S0263034613000104

Effects of laser profiles on fast electron generation under the same laser energy

M. HATA,[1] H. SAKAGAMI,[2] T. JOHZAKI,[3] AND H. NAGATOMO[4]

[1]Department of Physics, Nagoya University, Nagoya, Japan
[2]Fundamental Physics Simulation Research Division, National Institute for Fusion Science, Toki, Japan
[3]Mechanical Systems Engineering, Hiroshima University, Higashihiroshima, Japan
[4]Institute of Laser Engineering, Osaka University, Suita, Japan

(RECEIVED 28 November 2012; ACCEPTED 6 February 2013)

Abstract

In fast ignition, optimization of laser profile for core heating is one approach to ignite the core. However, the profile is not so optimized and its effects on fast electron characteristics are not fully clarified yet. The laser profile is optimized under the condition of same laser energy because laser energy is restricted in experiments. Therefore, we investigate effects of laser profile on fast electron generation under the condition of same laser energy. In this paper, each effect of laser temporal and spatial profile is estimated independently using two-dimensional Particle-In-Cell simulations. We conclude that lower intensity laser suitable for fast ignition under the limit of simulated parameters when energy of laser is same because efficient core-heating electrons are much generated and divergence angle is smaller in low-intensity case compared to high-intensity case.

Keywords: Fast electron generation; Fast ignition; laser profiles; Particle-in-cell

1. INTRODUCTION

A fast ignition scheme, in which the heating process is separated from the compression procedure, is expected to save driver energy and realize high gain fusion (Tabak *et al*., 1994). In this scheme, there are various methods to ignite a compressed core, for example a fast electron beam, a proton beam, shock wave, and so on (Tabak *et al*., 1994; Roth *et al*., 2001; Murakami *et al*., 2006). Many studies related with these methods have been performed from the proposal of the fast ignition scheme (Wilks *et al*., 1992; Beg *et al*., 1997; Pukhov & Vehn, 1997; Pukhov *et al*., 1999; Tabak *et al*., 2005; Key, 2007; Norreys *et al*., 2009). In Japan, the experiments using cone-guided targets, where the fast electron beam is used to ignite the core, were performed and the high temperature of about 1keV was achieved in 2002 (Kodama *et al*., 2002). As the next step, fast ignition realization experiments project phase-I (FIREX-I) (Azechi & The FIREX Project, 2006) has started at Institute Laser Engineering (ILE), Osaka university. The goal of FIREX-I is to demonstrate the ignition temperature of 5–10 keV by laser for fast ignition experiment (LFEX) that is four-beam bundled high-energy petawatt (10 kJ/10 ps) laser (Miyanaga *et al*., 2006). The first integrated experiments using the LFEX laser were done in 2009 (Mima *et al*., 2010), where the LFEX laser was operated with one-beam and low-energy mode, and integrated experiments by two-beam LFEX laser were performed in 2010 (Shiraga *et al*., 2011). Cone-guided targets are used in this project and the design optimization of the target has been performed and on going (Nakamura *et al*., 2008; Sakagami *et al*., 2009; Johzaki *et al*., 2011; Hata *et al*., 2012). In contrast, the laser profile is not so optimized and its effects on fast electron characteristics are not fully clarified yet. Therefore, it is necessary for complete optimization to investigate an influence of laser temporal and spatial profiles on them. According to the FIREX-I experiments in 2010, the intensity of the LFEX laser is about 1.0×10^{19} and its pulse length is 1 ps. Therefore, assuming these range of the intensity and pulse length, we investigate effects of laser temporal profile on fast electron generation using two-dimensional relativistic particle-in-cell code. In addition, we simulate effects of laser spatial profile on fast electron generation although it is small-scale simulation because of the restriction on computer power and resources. To refer our work for a guideline of optimization, we perform simulations under the same laser energy because the laser profile must be optimized under the condition of the same laser energy in the experiments.

Address correspondence and reprint requests to: M. Hata, Department of Physics, Nagoya University, Nagoya 464-8602, Japan. E-mail: hata.masayasu@nifs.ac.jp

2. EFFECTS OF LASER TEMPORAL PROFILE

In this section, laser-plasma interaction in the case of normal incidence to planar target is simulated and effects of laser temporal profile on fast electron characteristics under the same laser energy are investigated.

2.1. Simulation Condition

A prepulse of a heating laser is high intense (e.g., 10^{11} Wcm^{-2}) enough to create the plasma as the intensity of a main pulse is extremely high (e.g., 10^{19} Wcm^{-2}) even if the contrast ratio is 10^{8} (Sunahara *et al.*, 2012). Therefore, generation of a preformed plasma is unavoidable although some efforts are expended to avoid the preformed plasma generation (Sunahara *et al.*, 2012; Sakagami *et al.*, 2011).

Figure 1 shows (a) laser temporal profiles in four simulated cases and (b) two-dimensional profile of electron density of the target plasma. The gold-cone tip after prepulse irradiation is introduced as 36 μm thickness in x direction, 20 n_{cr}, real mass and $Z = 40$ plasma with preformed gold plasma, which has exponential profile of the scale length $L = 4$ μm with the density from 0.1to $20n_{cr}$, where n_{cr} is the critical density. The density profile in y direction is uniform and the width of the target is 16 μm. Laser beam irradiates the target at normal incidence and its spatial beam profile in y direction is uniform. To investigate effects of laser temporal profile on fast electron generation, we use four different temporal profiles that are combination of two maximum intensities (1.0×10^{20} and 2.5×10^{19} Wcm^{-2}) and two pulse shapes (flattop and gaussian) as summarized in Table 1. Pulse lengths are adjusted to preserve the laser energy. The intensity in the case of the flattop pulses rises up as a gaussian with half-width at half maximum (HWHM) of 4.7 fs, is kept constant with its corresponding maximum intensity during 90 or 390 fs, and falls down as the gaussian with same HWHM. The former is called FH (flattop of high-intensity) and the latter FL (Flattop of Low-intensity). In other two cases, the intensity profile is gaussian with HWHM of 47 or 188 fs and the first is called GH (Gaussian of high-intensity) and the second GL (gaussian of low-intensity). Boundary conditions in x direction are reflection for particles and perfect absorption for electromagnetic waves. In y direction, periodic boundary conditions are applied for both particles and electromagnetic waves. Under these conditions, simulations are performed for 2000 fs and fast electrons that pass through the vertical line 5 μm behind the boundary between the preplasma and the flat profile plasma are observed. To ignore the circulation of fast electrons, fast electrons are artificially cooled down to initial temperature in the rear part, 6 μm from the rear edge of the plasma.

Table 1. *Maximum intensities and temporal shapes of laser*

Case	Maximum intensity	Temporal shape	
	$I[\mathrm{Wcm}^{-2}]$	$\tau_{rise/fall}$[fs]	τ_{flat}[fs]
FH (Flattop of High intensity)	1.0×10^{20}	4.7	90
FL (Flattop of Low intensity)	2.5×10^{19}	4.7	390
GH (Gaussian of High intensity)	1.0×10^{20}	47	0
GL (Gaussian of Low intensity)	2.5×10^{19}	188	0

2.2. Fast electron characteristics: Energy spectra

Time-integrated energy spectra of fast electrons for the four cases are shown in Figure 2. In both pulse shapes, low-energetic electrons (<7 MeV) decrease, and high-energetic electrons (>7 MeV) are more generated as the laser intensity becomes high. According to some scaling laws (Wilks *et al.*, 1992; Beg *et al.*, 1997; Pukhov *et al.*, 1999; Haines *et al.*, 2009), the slope temperature of generated electrons is approximately proportional to the value between the square root and cube root of the laser intensity. Slope temperatures between 5 and 20 MeV in the four cases are summarized in Table 2. Ratios between the temperatures of high- and low-intensity lasers in the flattop and gaussian cases T_H/T_L are 1.5 and 1.63, respectively, and they approximately agree with that in scaling law of the cube root, namely $(I_H/I_L)^{1/3} = 1.59$. Energy coupling efficiencies from the laser to observed electrons with energies of all range, less than 0.2, 0.2–2, 2–7 MeV, and more than 7 MeV are calculated and summarized in Table 2. Though the difference on coupling efficiencies to whole observed electrons among all cases is approximately 20% at most, there is not so much difference compared to that at range of each energy. Therefore, if the scaling law is applied to each cases, low-energy electrons are less generated,

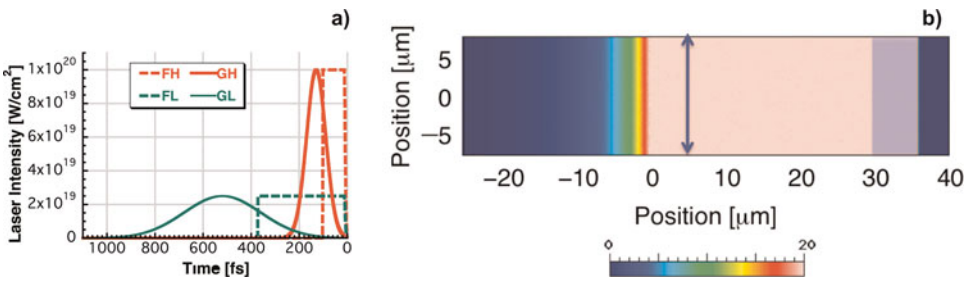

Fig. 1. (Color online) (**a**) Laser temporal profiles in four simulated cases and (**b**) two-dimensional profile of electron density of the target plasma, where blue line indicates the line for observation and blue shade in rear plasma represents artificially cooling region.

https://doi.org/10.1017/S0263034613000104 Published online by Cambridge University Press

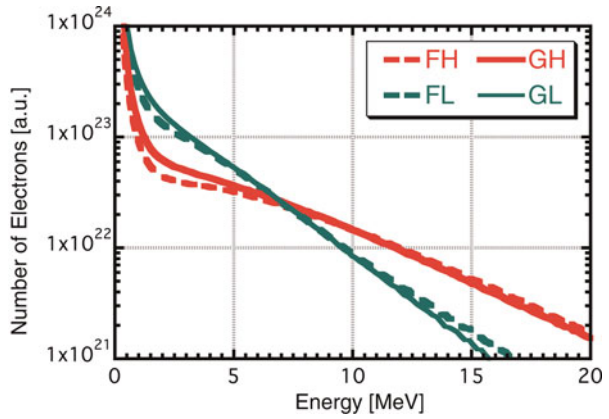

Fig. 2. (Color online) Time-integrated energy spectra of fast electrons, where red and green lines mean high- and low-intensities and dashed and solid lines indicate flattop and gaussian cases, respectively.

the number of high-energy electrons increases in the high-intensity case compared to the low-intensity case, and intersection points of electron energy spectra probably appear as shown in Figure 2. In the scaling law, generated fast electrons have the effective slope temperature, so, it is assumed that energy distribution function of these electrons is expressed by following equation:

$$f(E) = A\exp\left(-\frac{E}{T}\right), \tag{1}$$

where A and T are normalized coefficient and the effective temperature, respectively. Total energy of these electrons E_{tot} is given by

$$E_{\mathrm{tot}} = \int_0^\infty Ef(E)\mathrm{d}E. \tag{2}$$

When it is assumed that total energies are the same on two cases namely case 1 and 2, the energy at the intersection point of two equations, $E_{1,2}$ is given by

$$E_{1,2} = \frac{T_1T_2}{T_1 - T_2}\log\left(\frac{T_1^2}{T_2^2}\right). \tag{3}$$

Then, we can derive intersection points among all cases using effective temperatures given in Table 2, i.e., $E_{\mathrm{FH,FL}}$, $E_{\mathrm{GH,GL}}$ = 7.0, 6.8 MeV. Assuming same coupling efficiencies, calculated intersection points appear near 7 MeV in the scope of simulated intensities. Even if it takes different coupling efficiencies in consideration, only the term η_2/η_1 is multiplied to inside the logarithm in Eq. (3), where η is the coupling efficiency from the laser to electrons, and intersection points also appear near the 7 MeV. Therefore, energy spectra of generated fast electrons are approximately obtained using the scaling law if the coupling efficiencies from the laser to electrons are given.

When the cases of same maximum intensities are compared in Figure 2, the generation of high energy electrons is narrowly enhanced and that of low-energy electrons is barely weakened in the case of flattop compared to the gaussian case because the lower intensity laser in the gaussian case irradiates longer than that in the flattop case. The difference of 0.2–2 MeV electrons in Table 2 is especially large compared to others and these electrons efficiently heat the core. Therefore, the GL case is clearly the most suitable for fast ignition in those parameters when laser energy is same.

2.3. Fast electron characteristics: Divergence angle

It is important for a evaluation of core heating to investigate the divergence angle of fast electrons. Electron angular distribution is composed from observed electron data and HWHMs of the angular distribution in both cases are calculated and shown as afunction of electron energy in Figure 3. In both cases, the divergence angle in the high-intensity case is larger than that of the low-intensity case because high intensity laser generates large electron currents, they induce large magnetic fields, and the strong scattering of electrons occurs. Figure 4 shows time evolutions of maximum magnetic field in the cases of flattop and gaussian. Strong magnetic fields that easily bend the path of MeV electrons are observed in both high- and low-intensity cases. Although these magnetic fields scatter generated fast electrons, high energetic fast electrons are not affected so much because of the high energy. On the other hand, low-energetic electrons are enough to be affected and their divergence angles are similar in all cases, therefore, the divergence angle of 0–2 MeV electrons are almost the same among all cases. Furthermore, initially generated electrons has small divergence angle because of no magnetic fields. Therefore, divergence

Table 2. *Slope temperatures and coupling efficiencies from laser to observed electrons with energies of all range, less than 0.2, 0.2–2, 2–7 MeV, and more than 7 MeV*

Case	T_e [MeV]	Coupling efficiencies of each electron energy range [%]				
		All range	<0.2 MeV	0.2–2 MeV	2–7 MeV	7 MeV<
FH	4.5	71.96	9.20	5.44	18.50	38.83
FL	3.0	82.28	13.02	16.67	33.41	19.19
GH	4.4	78.49	11.36	8.65	21.87	36.62
GL	2.7	86.41	12.01	21.18	35.74	17.48

https://doi.org/10.1017/S0263034613000104 Published online by Cambridge University Press

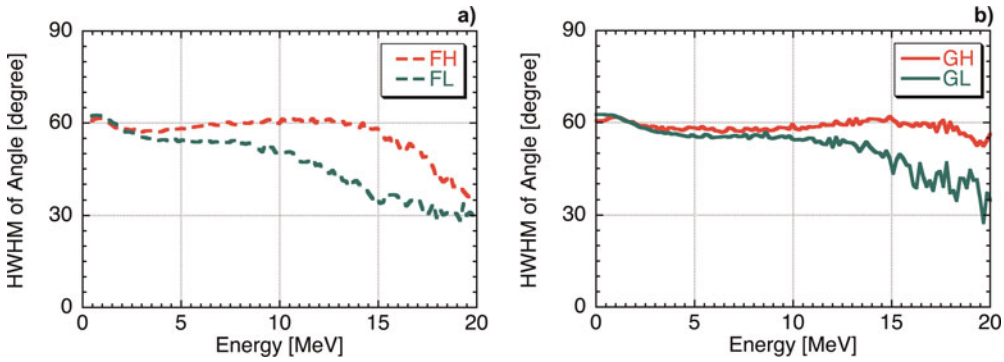

Fig. 3. (Color online) HWHMs of angle as a function of electron energy in the cases of (**a**) flattop and (**b**) gaussian, where red and green lines indicate high- and low-intensities and dashed and solid lines indicate flattop and gaussian, respectively.

angle in the case of flattop becomes small compared to the Gaussian case because many electrons are initially generated.

Consequently, divergence angles of high-energetic fast electrons vary with the laser intensity, however those of low-energetic fast electrons are similar in spite of the laser intensity because of large magnetic fields. From the standpoint of the fast ignition, there is no difference because the divergence angles of 0–2 MeV electrons that efficiently heat the core are almost the same, however, it is serious problem that the divergence angle is much large in whole simulated cases.

3. EFFECTS OF LASER SPACIAL PROFILE

In this section, simulations of laser plasma interaction are performed varying laser spacial profile under the same laser energy and its effects on fast electron characteristic are investigated.

3.1. Simulation Condition

Figure 5 shows spatial profiles of laser in two simulated cases and two-dimensional profile of electron density of target plasma. Target conditions are similar to previous simulations, but some parameters are different. The thickness (in x direction) of the gold-cone tip is 15 μm because of the reduction of simulation time. The width (in y direction) of the target plasma is set to 70 μm that is more than three times as large as laser spot sizes. The temporal profile of the laser beam is flattop and the pulse length is semi-infinite. We use two spatial profiles, namely gaussian with the spot diameter of 10 μm and the intensity of 1×10^{20} Wcm^{-2} and gaussian with 20 μm and 5×10^{19} Wcm^{-2} as shown in Figure 5. Spot diameters are adjusted to preserve the total laser energy. Each profile is named G10 and G20, respectively. Boundary conditions are reflection for particles and perfect absorption for electromagnetic waves in both x and y directions. As shown in Figure 5b, cooling region (blue shade) for avoiding the circulation of fast electrons are set in the regions of $10 < x < 15$ and $-30 < y < 30$ μm, $0 < x < 10$ and $30 < y < 35$ μm, and $0 < x < 10$ and $-35 < y < -30$ μm, where $x = 0$ μm is defined at boundary between the preformed plasma and the gold-cone tip and $y = 0$ μm at the center of the target. Under these conditions, simulations are performed for 200 fs and passing fast electrons are observed at the area of $x = 5$ μm and $y = 0$–25 μm.

3.2. Fast electron characteristics: Beam intensity

Figure 6 shows time-evolutions of the electron beam intensity at $y =$ (a) 0–5, (b) 10–15, and (c) 20–25 μm. In both cases of G10 and G20, the electron beam intensity is high near the laser axis and becomes low as the laser intensity at the area for observation is lower. At $y = 0$–5 μm, the electron beam intensity in the G10 case exceeds that in the G20 case because the laser intensity of the G10 case at this region is higher than that of the G20 case as shown in Figure 5.

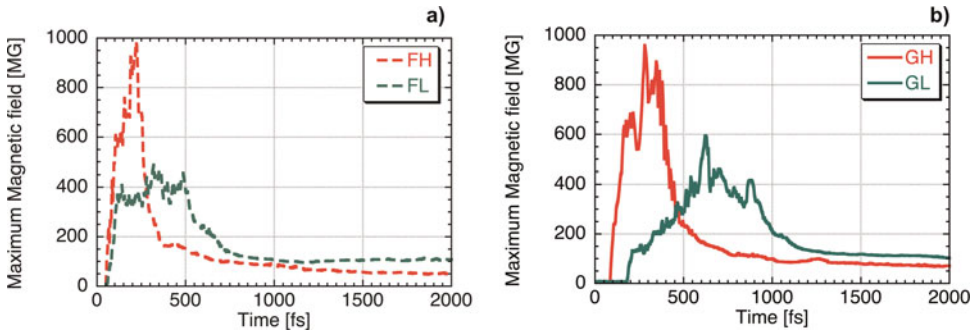

Fig. 4. (Color online) Time evolutions of maximum magnetic field inside the plasma in the cases of (**a**) flattop and (**b**) gaussian, where red and green lines indicate high- and low-intensities and dashed and solid lines indicate flattop and gaussian, respectively.

https://doi.org/10.1017/S0263034613000104 Published online by Cambridge University Press

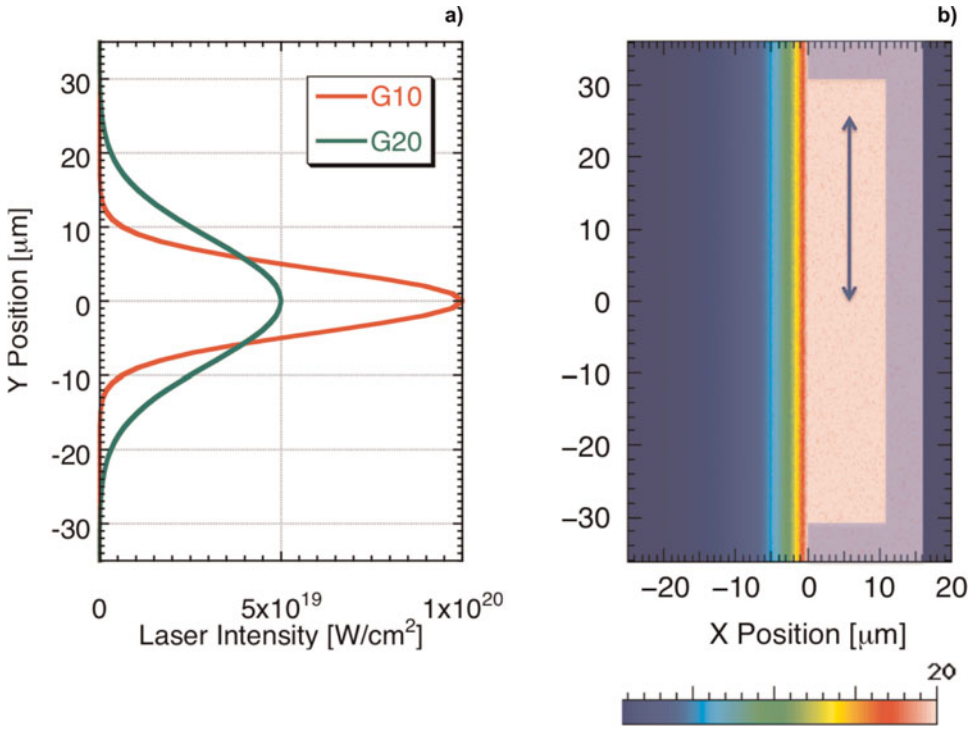

Fig. 5. (Color online) Spatial profiles of laser in two simulated cases and two-dimensional profile of electron density of target plasma, where blue arrow indicate the line for observation and blue shade in rear plasma represents artificially cooling region.

At $y = 20$–25 μm, the electron beam intensity in the G20 case is higher than that in the G10 case, because the relationship of the laser intensity is reversed. However the difference of the electron beam intensity is not large compared to that of the laser intensity as most of electrons are come from the region where the laser intensity is high. In the G10 case, the time at which the electron beam intensity rises is later than that in the G20 case. It implies that observed electrons are come from another region, namely near the laser axis. At $y = 10$–15 μm, there are not much differences on time

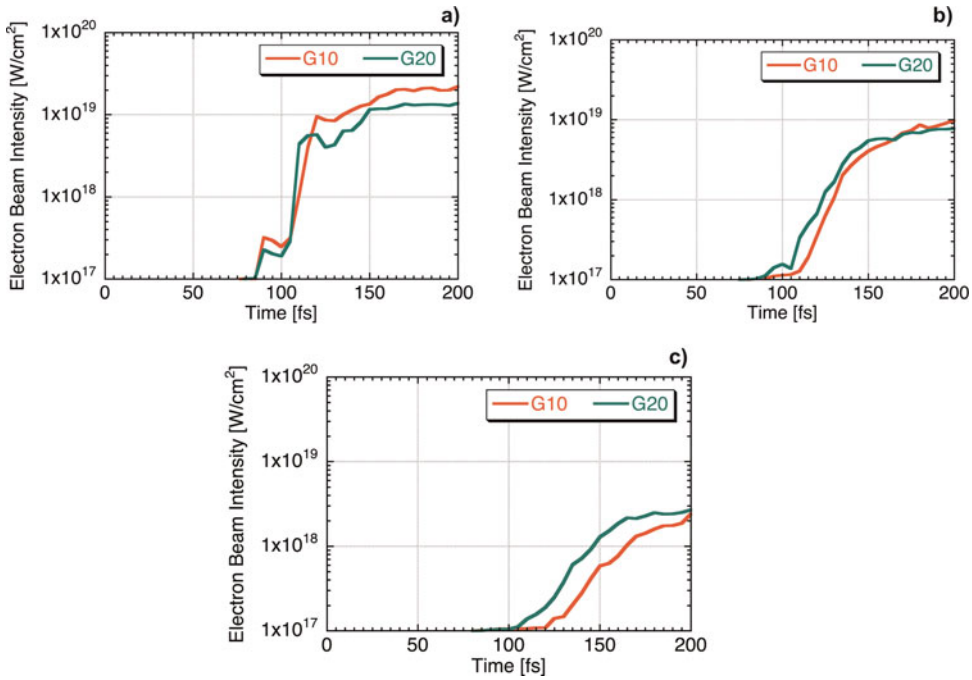

Fig. 6. (Color online) Time-evolutions of the electron beam intensity at $y =$ (**a**) 0–5, (**b**) 10–15, and (**c**) 20–25 μm, where red and green lines indicate G10 and G20 cases, respectively.

https://doi.org/10.1017/S0263034613000104 Published online by Cambridge University Press

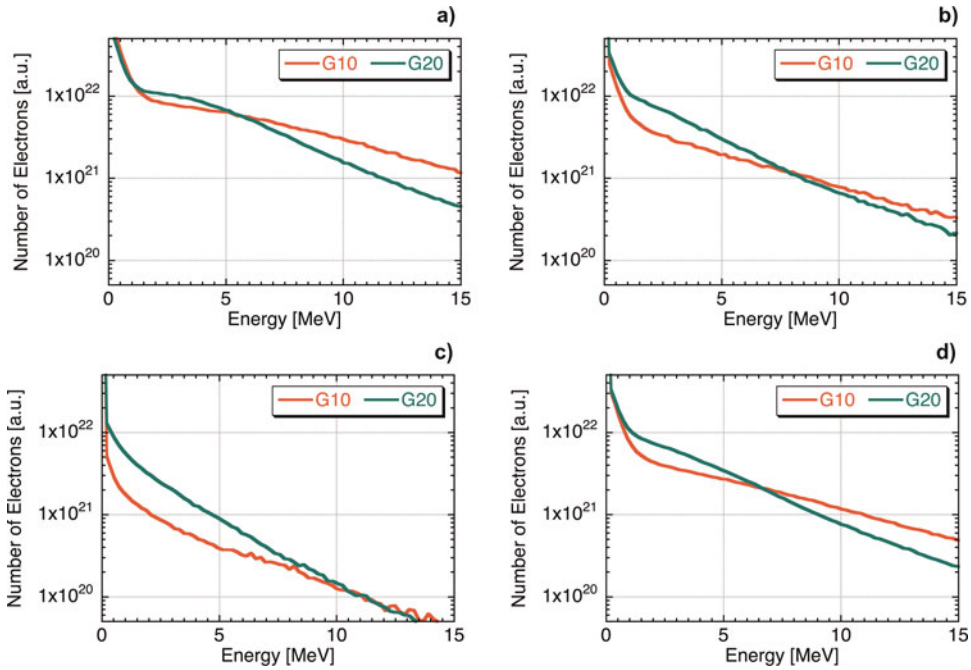

Fig. 7. (Color online) Time-integrated electron energy spectra at $y =$ (**a**) 0–5, (**b**) 10–15, (**c**) 20–25, and (**d**) 0–25 μm, where red and green lines indicate G10 and G20 cases, respectively.

evolutions of the electron beam intensity and the rising time in the G10 case is also later than that in the G20 case. Consequently, electron beam intensities normally reflect the laser intensity in each area although the contribution from another area is not negligible.

3.3. Fast electron characteristics: Energy spectra

Figure 7 shows time-integrated electron energy spectra in the G10 and G20 cases at $y =$ (a) 0–5, (b) 10–15, (c) 20–25, and (d) 0–25 μm. At each area, the slope temperature in the G10 case is higher than that in the G20 case. As the observed area is far from the laser axis, number of fast electrons decreases. Its variation in the G10 case is the larger than that in the G20 case because the laser intensity in the G10 case is rapidly damped with the distance from the laser axis compared to the G20 case. At $y =$ 0–25 μm, low-energetic electrons (<6.5 MeV) decrease and high-energetic electrons (>6.5 MeV) are more generated as the laser intensity becomes high. In Figure 7d, slope temperatures in the cases of G10 and G20 are 6.0 and 3.7 MeV, respectively. The estimated slope temperatures are between 1.5 and 15 MeV. The ratio of two slope temperature is 1.62 and it agree with scaling law of the cube root. If we pay attention to energy spectra of generated fast electrons, the G20 case is suitable for fast ignition because low-energetic electrons are much generated.

3.4. Fast electron characteristics: Divergence angle

To evaluate divergence angle, HWHMs of the angular distribution that is composed from observed electron data at $y =$ 0–25 μm are calculated and shown as a function of electron energy in Figure 8. In both cases, HWHMs of high-energetic electrons (>10 MeV) are small compared to those of low-energetic electrons (<10 MeV). HWHMs in the G10 case are larger than those in the G20 case. Green *et al.* (2008) reported that effects of focal spot are small and the divergence angle strongly depends on the laser intensity in 2008. Furthermore, according to Two dimensional PIC simulations in that research, divergence angles of whole observed electrons for different intensities of 1×10^{20} and 2×10^{19} Wcm^{-2} in the case of 16 μm focal spot diameter are 35 and 45, respectively. Our results are consistent with that research although we vary both parameters of focal spot diameter and laser intensity simultaneously because of the same

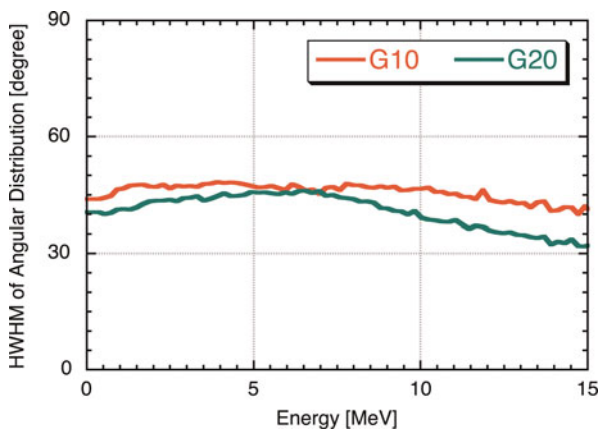

Fig. 8. (Color online) HWHMs of the angular distribution, where red and green lines indicate G10 and G20 cases, respectively.

https://doi.org/10.1017/S0263034613000104 Published online by Cambridge University Press

laser energy. These results show that the G20 case is more suitable for fast ignition because of smaller divergence angle.

4. SUMMARY

We performed two kind of simulations. One is for investigating the effects of the laser temporal profiles on fast electron generation and another one is for that of the spatial profiles. In each simulation, we fixed laser energy because we must optimize laser profile under the condition of the same laser energy in experiments. In effects of temporal profiles, it is shown that lower intensity laser is suitable for fast ignition because low-energetic electrons that heat the core efficiently are much generated. Divergence angles of these electrons are similar in spite of the laser intensity because induced quasi static magnetic fields are enough large to scatter these electrons. In effects of spatial profiles, low-energetic electrons are much generated and divergence angles of these electrons are small in the case of the low-intensity case compared to the high-intensity case. In conclusion, temporally and spatially lower intensity laser is suitable for fast ignition in this study. However, we could not find lower limit of the laser intensity because large scale simulations are needed. They are remained as future study. Of course, each effect is estimated independently in this work, but their comparison and evaluation of coupled effects are needed for optimization of laser profiles. Further it must be considered that the pulse length and spot diameter are restricted by the confinement time and the size of the core for the optimization. These will be considered as a part of future study.

REFERENCES

Azechi, H. & The FIREX Project. (2006). Present status of the FIREX programme for the demonstration of ignition and burn. *Plasma Phys. Cont. Fusion* **48**, B267–B275.

Beg, F., Bell, A., Dangor, A., Danson, C., Fews, A., Glinsky, M., et al. (1997). A study of picosecond laser-solid interactions up to 10^{19} W/cm^2. *Phys. Plasmas*, **4**, 447.

Green, J., Ovchinnikov, V., Evans, R., Akli, K., Azechi, H., Beg, F., et al. (2008). Effect of laser intensity on fast-electron-beam divergence in solid-density plasmas. *Phys. Rev. Lett*., **100**, 15003.

Haines, M., Wei, M., Beg, F. & Stephens, R. (2009). Hot-electron temperature and laser-light absorption in fast ignition. *Phys. Rev. Lett*., **102**, 45008.

Hata, M., Sakagami, H., Sunahara, A., Johzaki, T. & Nagatomo, H. (2012). Effects of ch foam preplasma on fast ignition. *Laser Part. Beams* **30**, 189–197.

Johzaki, T., Nagatomo, H., Sunahara, A., Cai, H., Sakagami, H., Nakao, Y., et al. (2011). Pre-plasma effects on core heating and enhancing heating efficiency by extended double cone for firex. *Nucl. Fusion* **51**, 073022.

Key, M. (2007). Status of and prospects for the fast ignition inertial fusion concept. *Phys. plasmas* **14**, 055502.

Kodama, R., Shiraga, H., Shigemori, K., Toyama, Y., Fujioka, S., Azechi, H., et al. (2002). Nuclear fusion: fast heating scalable to laser fusion ignition. *Nat*. **418**, 933–934.

Mima, K., Sunahara, A., Shiraga, H., Nishimura, H., Azechi, H., Nakamura, T., et al. (2010). Firex project and effects of self-generated electric and magnetic fields on electron-driven fast ignition. *Plasma Phys. Contr. Fusion* **52**, 124047.

Miyanaga, N., Azechi, H., Tanaka, K., Kanabe, T., Jitsuno, T., Kawanaka, J., et al. (2006). 10-kj pw laser for the firex-i program. *Phys*. **133**, 81–87.

Murakami, M., Nagatomo, H., Azechi, H., Ogando, F., Perlado, M. & Eliezer, S. (2006). Innovative ignition scheme for ICFimpact fast ignition. *Nucl. Fusion* **46**, 99.

Nakamura, T. Mima, K., Sakagami, H., Johzaki, T. & Nagatomo, H. (2008). Generation and confinement of high energy electrons generated by irradiation of ultra-intense short laser pulses onto cone targets. *Laser Part. Beams* **26**, 207–212.

Norreys, P., Scott, R., Lancaster, K., Green, J., Robinson, A., Sherlock, M., et al. (2009). Recent fast electron energy transport experiments relevant to fast ignition inertial fusion. *Nucl. Fusion* **49**, 104023.

Pukhov, A., Sheng, Z. & Meyer-Ter-Vehn, J. (1999). Particle acceleration in relativistic laser channels. *Phys. Plasmas* **6**, 2847–2854.

Pukhov, A. & Vehn, J. Meyer-ter. (1997). Laser hole boring into overdense plasma and relativistic electron currents for fast ignition of icf targets. *Phys. Rev. Lett*., **79**, 2686–2689.

Roth, M., Cowan, T., Key, M., Hatchett, S., Brown, C., Fountain, W., et al. (2001). Fast ignition by intense laser-accelerated proton beams. *Phys. Rev. Lett*., **86**, 436–439.

Sakagami, H., Johzaki, T., Nagatomo, H. & Mima, K. (2009). Generation control of fast electron beam by low-density foam for firex-i. *Nucl. Fusion* **49**, 075026.

Sakagami, H., Sunahara, A., Johzaki, T. & Nagatomo, H. (2011). Effects of long rarefied plasma on fast electron generation for firex-i targets. *Laser Part. Beams* **30**, 103.

Shiraga, H., Fujioka, S., Nakai, M., Watari, T., Nakamura, H., Arikawa, Y., et al. (2011). Fast ignition integrated experiments with gekko and lfex lasers. *Plasma Phys. Contr. Fusion* **53**, 124029.

Sunahara, A., Johzaki, T., Nagatomo, H. & Mima, K. (2012). Generation of pre-formed plasma and its reduction for fast-ignition. *Laser Part. Beams*, **30**, 95.

Tabak, M., Clark, D., Hatchett, S., Key, M., Lasinski, B., Snavely, R., et al. (2005). Review of progress in Fast Ignition. *Phys. Plasmas*, **12**, 057305.

Tabak, M., Hammer, J., Glinsky, M.E., Kruer, W.L., Wilks, S.C., Gampbell, E.M., et al. (1994). Ignition and high gain with ultrapowerful lasers. *Phys. Plasmas* **1**, 1626–1634.

Wilks, S., Kruer, W., Tabak, M. & Langdon, A. (1992). Absorption of ultra-intense laser pulses. *Phys. Rev. Lett*. **69**, 1383–1386.

https://doi.org/10.1017/S0263034613000104 Published online by Cambridge University Press